Applied
Ceramic
TECHNOLOGY
International Journal of

SPECIAL ISSUE ARTICLE

Experimental evaluation and theoretical prediction of elastic properties and failure of C/C-SiC composite

Yuan Shi[1] | Shuguang Li[2] | Elena Sitnikova[2] | Daniel Cepli[1] | Dietmar Koch[3]

[1]Institute of Structures and Design, German Aerospace Center Stuttgart, Stuttgart, Germany

[2]Faculty of Engineering, University of Nottingham, Nottingham, UK

[3]Institute of Materials Resource Management, University of Augsburg, Augsburg, Germany

Correspondence
Yuan Shi, Institute of Structures and Design, German Aerospace Center Stuttgart, Pfaffenwaldring 38-40, 70569 Stuttgart, Germany.
Email: yuan.shi@dlr.de

Abstract

The paper presents experimental characterization and theoretical predictions of elastic and failure properties of continuous carbon fiber reinforced silicon carbide (C/C-SiC) composite fabricated by Liquid Silicon Infiltration (LSI). Its mechanical properties were determined under uniaxial tensile, compression, and pure shear loads in two sets of principal coordinate systems, 0°–90° and ±45°, respectively. The properties measured in the 0°–90° coordinate system were employed as the input data to predict their counterparts in the ±45° coordinate system. Through coordinate transformations of stress and strain tensors, the elastic constants and stress-strain behaviors were predicted and found to be in good agreement with the experimental results. In the same way, three different failure criteria, maximum stress, Tsai-Wu, and maximum strain, have been selected for the evaluation of the failure of C/C-SiC as a type of genuinely orthotropic material. Based on the comparisons with experimental results, supported by necessary practical justifications, the Tsai-Wu criterion was found to offer a reasonable prediction of the strengths, which can be assisted by the maximum stress criterion to obtain an indicative prediction of the respective failure modes.

KEYWORDS
C/C-SiC, ceramic matrix composites, failure, mechanical properties, modeling/model

1 | INTRODUCTION AND OBJECTIVE

Due to its excellent mechanical properties, favorable damage tolerance and comparatively low density, continuous carbon fiber reinforced carbon silicon carbide (C/C-SiC) composite fabricated by Liquid Silicon Infiltration (LSI) process has been successfully used in aerospace, energy, and transport technology.[1-8] The preliminary investigation of siliconization in German Aerospace Center Stuttgart started in the late 1980s and the manufacturing process of LSI-based C/C-SiC was developed in the beginning of 2000s.[9] Since then, material properties of the composite have been characterized intensively. The in-plane and out-of-plane mechanical properties under different loads, thermal properties and the effect of high temperature were investigated and summarized in Ref. [10] The strength ratio between bending and tensile load was approx. 1.7–2.0 depending on the different loading directions.[11] The acoustic emission (AE) technique has been used for the determining the relationship between its tensile strength and damage-related AE energy.[12] Based on the statistical analysis, strength values under tensile, compression and bending loads can be described using normal or Weibull

---

distribution for each of the various failure mechanisms.[13] Hofmann[14] has developed a finite element approach based on the cohesive-zone-elements for the modelling of mechanical behaviors of C/C-SiC with interlaminar defects, which is validated by comparing the numerical and three-point bending results of delaminated samples. The elastic properties of wound C/C-SiC with different winding angles can be calculated through the input data of equivalent UD-ply, which was computed by Inverse Laminate Theory.[15] The damage-based failure criteria were proposed for the modelling of inelastic behavior of similar composites.[16,17] Furthermore, according to the in situ X-ray tomography characterization of LSI C/C-SiC, significant strain oriented in through-thickness direction and their localizations were observed at small applied stress.[18] However, some important mechanical properties of C/C-SiC, especially in $\pm45°$ direction, have still not been investigated in detail, and the appropriateness of various failure criteria for the prediction of strength under different loadings should be explored.

The objective of material characterization as described above was to prepare this type of materials so that they will become ready to be adopted in engineering structures. In practical applications, materials are usually expected to sustain loading conditions which will surely go beyond the stress states as employed to characterize the material, viz. uniaxial tension and compression and pure shear in materials principal axes. Almost inevitably, materials will be exposed to stress states where multiple components are present with their magnitude being comparable to their respective strengths. As the number of such stress states is inexhaustible, it is impossible to determine the strength experimentally for each stress state encountered. It is therefore essential to have some suitable failure criteria which would be capable of incorporating the effects of each individual stress component in assessing the safety of the material under a general combined stress state.

Failure criteria for composites have been a field which has attracted extensive attention from the composites' community since the emergence of modern high-performance composites. There have been dozens, if not more, of failure criteria of various kinds. Some of them have been reviewed and assessed in a series of well-organized world-wide round-robin exercises.[19-21] It is therefore not the intention of the present paper to re-present the findings out of these exercises. A fair observation is that most criteria available were proposed for unidirectionally (UD) fiber-reinforced composites, which can be reasonably assumed to be transversely isotropic. The C/C-SiC composite as is the interest of the present paper can be best described as laminates of a woven fabric reinforced composite (section 0) while each lamina involved is effectively a genuine orthotropic material. None of the criteria proposed specifically for UD composites is expected to be applicable to such a material. Among those applicable to genuine orthotropic materials are the maximum stress criterion, the

maximum strain criterion and the Tsai-Wu criterion. The first two are the most primitive ones extended from their respective counterparts for isotropic materials. According to,[22,23] the maximum strain criterion is logically less consistent than the maximum stress criterion, although some practitioners seemed to prefer the latter, likely due to historical reasons.[24] It has been demonstrated in Ref. [23] that, after a number of rational considerations based on the concept of 'effective strains' instead of 'apparent strains', the maximum strain criterion reproduces the outcomes of the maximum stress criterion and therefore is unified with the maximum stress criterion under the assumption of linear elasticity up to the failure. The accuracy of the maximum stress/strain criterion relies on the stress states being primarily uniaxial stress or pure shear in materials principal axes, in which case, their predictions are more or less a straightforward re-presentation of the input strengths or failure strains. Beyond these stress states, the accuracy of the predictions cannot be taken for granted.

The Tsai-Wu criterion[25-27] was one of the earlier attempts of incorporating the contributions of all stress components to the failure of the material and it was proposed within a framework applicable to genuine orthotropic materials, at least initially. However, its systematic applications as demonstrated in Ref [19,20] and rationalized in Ref [27] have been mostly limited to transversely isotropic materials. There have not been many completely sets of elastic and strength properties of genuinely orthotropic materials in the open literature, let alone their systematic applications in failure predictions. One of the objectives of this paper was to offer a complete set of material properties and their systematic applications.

Another attractive feature of this criterion was that it had covered a significant number of other failure criteria in this category such that they could be considered as special cases of it, for example, the Hoffmann criterion.[28] The criterion has been subject to a lot of admiring endorsements on one extreme and dismissive criticisms one the other. However, most of its appraisals, whether positive or negative, are subjective, and the common and seemingly compelling argument has been the agreement with experimental data. In fact, most of the experimental data in the open literature are incomplete and hence insufficient to support proper predictions using the Tsai-Wu criterion. Among the limited available number of complete sets of data, good and bad comparisons almost break even. The objectiveness of such comparisons is often questionable, as a careful and responsible experimentalist would agree that in the experimentally measured data, such as strengths or failure strains employed as the input for a failure criterion, the inaccuracies involved in experiments, even those devised following established industrial standards, can be as significant as the scatter present in some of the theoretical predictions. Typical sources of errors are the stress states in the specimen not being sufficiently uniform, or not being

sufficiently uniaxial or pure shear, and failure mechanisms being interfered by structural behaviors, such as edge effects, delamination, buckling, etc. where the actual failure is dominated by the highly localized stresses/strains.

A typical criticism of the Tsai-Wu criterion in the literature is its lack of representation of the failure modes in the criterion, for example, tensile, compressive, and shear. In other words, all failure modes are predicted by a single failure function reaching its critical value and some researchers find this unacceptable.

The failure analyses as presented in this paper, while being compared with available experimental data, will serve as some verifications from a specific perspective.

2 | MATERIAL AND EXPERIMENTAL

2.1 | Material C/C-SiC

The material to be investigated is C/C-SiC, a continuous carbon fiber reinforced ceramic composite with carbon and silicon carbide matrix. The so-called green plate was prepared by stacking several layers of 2/2 twill weave fabric of carbon fibers pre-infiltrated with phenolic resin as precursor (prepreg with 3 K HTA fibers of Teijin Carbon Europe GmbH, phenolic resin with about 60 mass% carbon and can provide a dimensionally stable structure after pyrolytic processes). In order to obtain overall orthotropy in the coordinate system defined by the fiber tow directions in the plane, the alternating layers of fabric were rotated by 90° during the ply stacking (Figure 1). The green plate was subsequently used to manufacture the C/C-SiC material through Liquid Silicon Infiltration (LSI) technology, and the LSI process can be subdivided in three main process steps: greenbody, pyrolysis, and siliconization. First, Carbon Fiber Reinforced Polymers (CFRP) preform was manufactured via warm pressing ($T_{max} = 240°C$, $P_{max} = 5.8$ kPa) using green plate. Next, the CFRP plate was pyrolyzed at a temperature above 1500°C under inert gas atmosphere (nitrogen) and the polymer matrix was transformed to an amorphous and porous carbon matrix (carbonization). The carbon fibers are densely embedded in the carbon matrix and a crack pattern

evolves in the C/C body. Finally, during the siliconization step silicon with a purity of 99.9% is melted at T_{max} of approx. 1650°C and the liquid silicon was infiltrated into the porous C/C structure by capillary forces and reacted with the carbon matrix to form silicon carbide. Because of the LSI method, the final C/C-SiC contains load bearing carbon fiber bundles which are embedded in a dense SiC matrix with a small amount of residual Si and C. The fiber volume content of C/C-SiC was calculated by the measurement of the initial weight of the carbon fibers and the total volume of the finished component. The density and open porosity of the manufactured plate material were measured using the Archimedes method.[29] The fiber volume content, open porosity and density of the C/C-SiC plates concerned are ~57.0%, 2.0%, and 2.0 g/cm^3, respectively.

The finished C/C-SiC material is shown in Figure 2 and the directions of x- and y-axis represent the fiber reinforcement orientations denoted as 0° & 90° instead of 0°/90° where the notation 0° & 90° refers to a block of paired layers of the woven fabrics as shown in Figure 1, whereas the 0°/90° notation as conventionally adopted in laminates made from UD plies often has a strong implication on the layer sequence. Since such a sequence is irrelevant for the composite concerned, the 0°/90° notation will be avoided in the present paper. Similarly, notation +45° & −45° is employed to refer to the 0° & 90° block but rotated by 45° in the plane of the composite. Use has also been made of notation 0°–90° and it is employed to refer to the principal axes of the material in these two directions of axes x–y. Similarly, notation ±45° is to refer to the directions of 1–2 coordinate axes as shown in Figure 2, which are 45° from axes x–y in the plane of the composite.

Assuming macroscopic homogeneity of the obtained ceramic matrix composite, it can be considered as a material instead of composite laminate. It is orthotropic in both sets of coordinate systems, 0°–90° (x- and y-axis) and ±45° (1- and 2-axis). Without the alternating layup arrangement (Figure 1), a twill weave is orthotropic only in the ±45° coordinate system, while there is nothing that supports its orthotropy categorization in the 0°–90° coordinate system as one's intuitive choice. Detailed argument can be found in Ref [30].
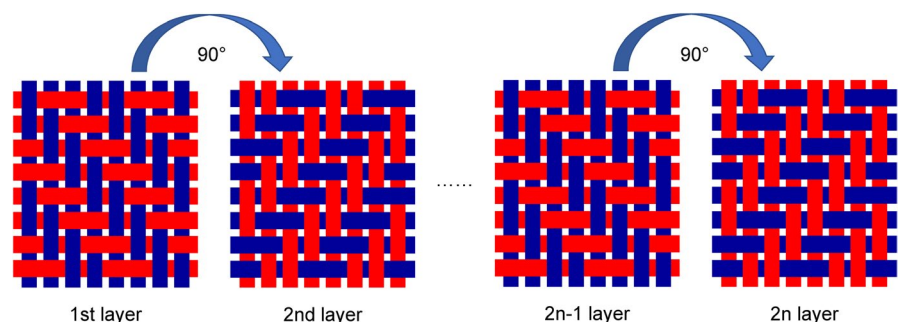

FIGURE 1 Preform and lamination of continuous HTA carbon fibers with 2/2 twill woven for the manufacturing of C/C-SiC

90°   90°

......

1st layer   2nd layer   2n-1 layer   2n layer

2.2 | Mechanical tests

The mechanical properties, including elastic and shear moduli (E and G), Poisson's ratio (ν), strength (σ), and failure strain (ε), of the investigated C/C-SiC material with different fiber orientations 0° & 90° and +45° & −45° were measured under uniaxial tensile, Iosipescu-shear, and uniaxial compression loading. The coupons for the tests were cut from flat plate with thicknesses of 3 mm. Table 1 gives an overview of the performed mechanical tests with the associated standards, specimen size and the loading direction relative to the specimen geometries.
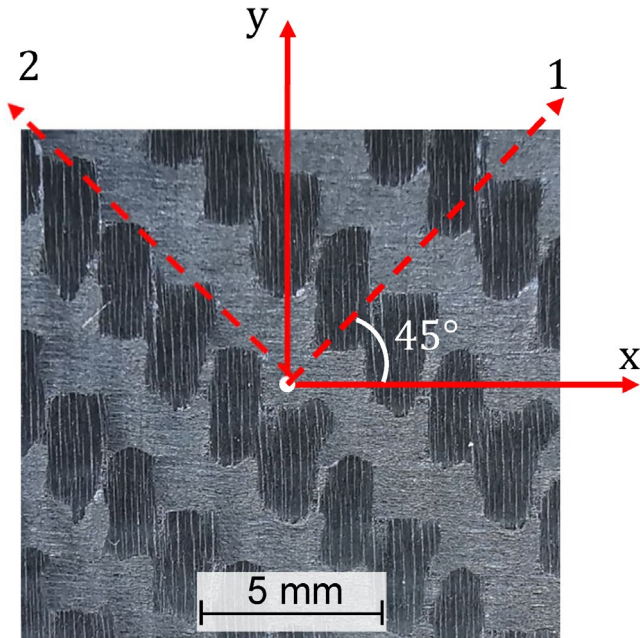

FIGURE 2 C/C-SiC material with fiber orientation of 0° & 90°, coordinate system (*x* and *y*-direction) in accordance with the mechanical loading directions and rotated to another coordinate system (1 and 2-direction) with rotation angle of 45°

All the experiments were performed up to failure on a universal testing machine (Zwick 1494) at a controlled cross head speed of 1 mm/min. For the displacement measurement the testing machine is equipped with extension measurement devices and the force and distance measured values are recorded synchronously. For the uniaxial tensile and compression tests, the longitudinal and transverse strains were measured with strain gauges. During Iosipescu-shear tests, the strains were evaluated using strain gauges in the +45° and −45° directions relative to the shear loading direction. For statistical confirmation at least three samples per series were tested.

3 | EXPERIMENTAL RESULTS

Figure 3 shows typical tensile, compressive, and shear stress-strain curves of the investigated C/C-SiC with fiber tow orientations 0° & 90° and +45° & −45°. The stress-strain response strongly depends on the loading direction. With 0° & 90° orientation and under uniaxial tensile and compression loading, the composite shows an almost linear behavior with higher stiffness and strength as seen in Figure 3, since the loading direction is aligned with one of the arrays of fiber tows. In contrast, under uniaxial tensile and compression loadings the composite with orientation of +45° & −45° shows non-linear behavior and stiffness and the strength values are considerably lower. This is so because the material is subject to a significant amount in-plane shear along the fibers, that is, in 0°–90° directions. As is well-known, in-plane shear behavior along fibers shows significant nonlinearity.[31] By contrast, a clear non-linear response in the Iosipescu-shear behavior of 0°&90° specimens with low shear modulus can be observed in Figure 3 as this is a problem dominated by the in-plane shear along fibers, which features nonlinearity as explained above. The Iosipescu-shear of the +45° & −45° specimens is rather linear, as is also shown in

TABLE 1 Specimen geometry with dimensions (thickness of 3 mm), loading direction for different mechanical tests and the associated standards

Test	Standard	Specimen geometries, dimensions, and loading direction
Uniaxial Tensile	DIN EN 658-1: 1999	
Iosipescu-shear	DIN EN 12289: 2005	
Uniaxial Compression	DIN EN ISO 20504:2020-01	

Figure 3, because dominating stresses in this case are tension in one family of fibers whilst compression in the other family and there is hardly any in-plane shear along fibers involved.

The mean value and standard deviation of C/C-SiC mechanical properties for both orientations under different loadings are summarized in Table 2. The determination of the Young's and shear moduli was conducted using a linear fit of the initial linear region of the stress-strain curves. E is the Young's modulus, ν is the Poisson's ratio and G the shear modulus. The indices x, y and 1, 2 correspond to the indications in Figure 2 and θ equals 45° for the fiber orientation +45° & −45°. The index T denotes the tensile test and C to the compression. Due to the symmetry of fiber orientation (Figure 1) the Young's modulus E_x is equal to E_y, and the values of E_1 and E_2 are theoretically identical, respectively. The failure stress was calculated from the maximum load according to the associated standards. The determined tensile and compression strengths σ
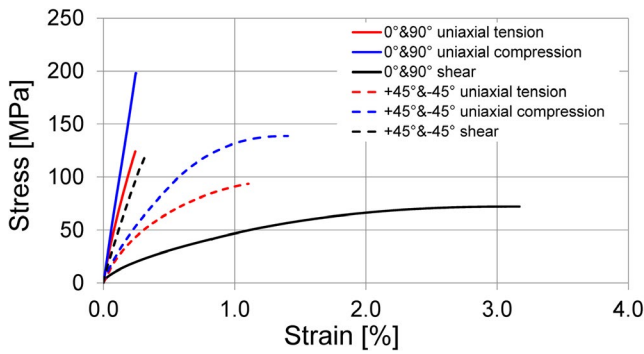
and shear strengths τ are listed in Table 2. The fracture strain ε under tensile or compression loading and γ of shear test was defined as the strain value at the related maximum strength, which are listed in Table 2 too. Similar to elastic values, the strength σ_x is equal to σ_y, σ_1 to σ_2 and ultimate strain ε_x to ε_y, ε_1 to ε_2, respectively. It should be noted that the mechanical properties of C/C-SiC with orientation 0°&90° have been published in the previous works[10,32] and they are included in Table 2 for completeness and ease of reference.

4 | DISCUSSION

4.1 | Failure modes

Figure 4 shows the typical failure modes of C/C-SiC specimens under investigation with fiber orientation 0° & 90° (Figure 4A–D) and +45° & −45° (Figure 4E–H). The indices x, y and 1, 2 correspond to the indications in Figure 2; z-(Figure 4C) and 3-axis (Figure 4G) denote the thickness direction of the samples with orientation of 0° & 90° and +45° & −45°, respectively. Just like their stress-strain behaviors, the failure modes depend strongly on the loading direction and fiber orientation.

Figure 4A shows the typical fracture mode due to uniaxial tension along the direction of one array of fiber tows whilst transverse to the direction of the other array of fiber tows. Clear fiber breakage is observed for the tows in the loading direction accompanied by matrix crack in or between the tows in the other direction. There is no obvious out-of-plane deformation over the fracture area and this is one of characteristics of tensile fracture of brittle materials in general.

FIGURE 3 Typical stress-strain behaviors of C/C-SiC material with fiber orientation of 0° & 90° and +45° & −45° under uniaxial tensile, compression, and pure shear loading

TABLE 2 Summary of elastic constants and fracture properties of material C/C-SiC with fiber orientation 0° & 90° and +45° & −45° obtained from tensile, compression, and Iosipescu-shear tests

Elastic constants				
	$E_x^T = E_y^T$ [GPa]	$E_x^C = E_y^C$ [GPa]	ν_{xy}^T [−]	G_{xy} [GPa]
0° & 90°	72.8 ± 2.1	74.4 ± 10.6	0.02 ± 0.01	9.5 ± 1.7
	$E_1^T = E_2^T$ [GPa]	$E_1^C = E_2^C$ [GPa]	ν_{12}^T [-]	G_{12} [GPa]
+45° & −45°	25.4 ± 1.3	26.8 ± 2.5	0.64 ± 0.02	42.7 ± 2.2

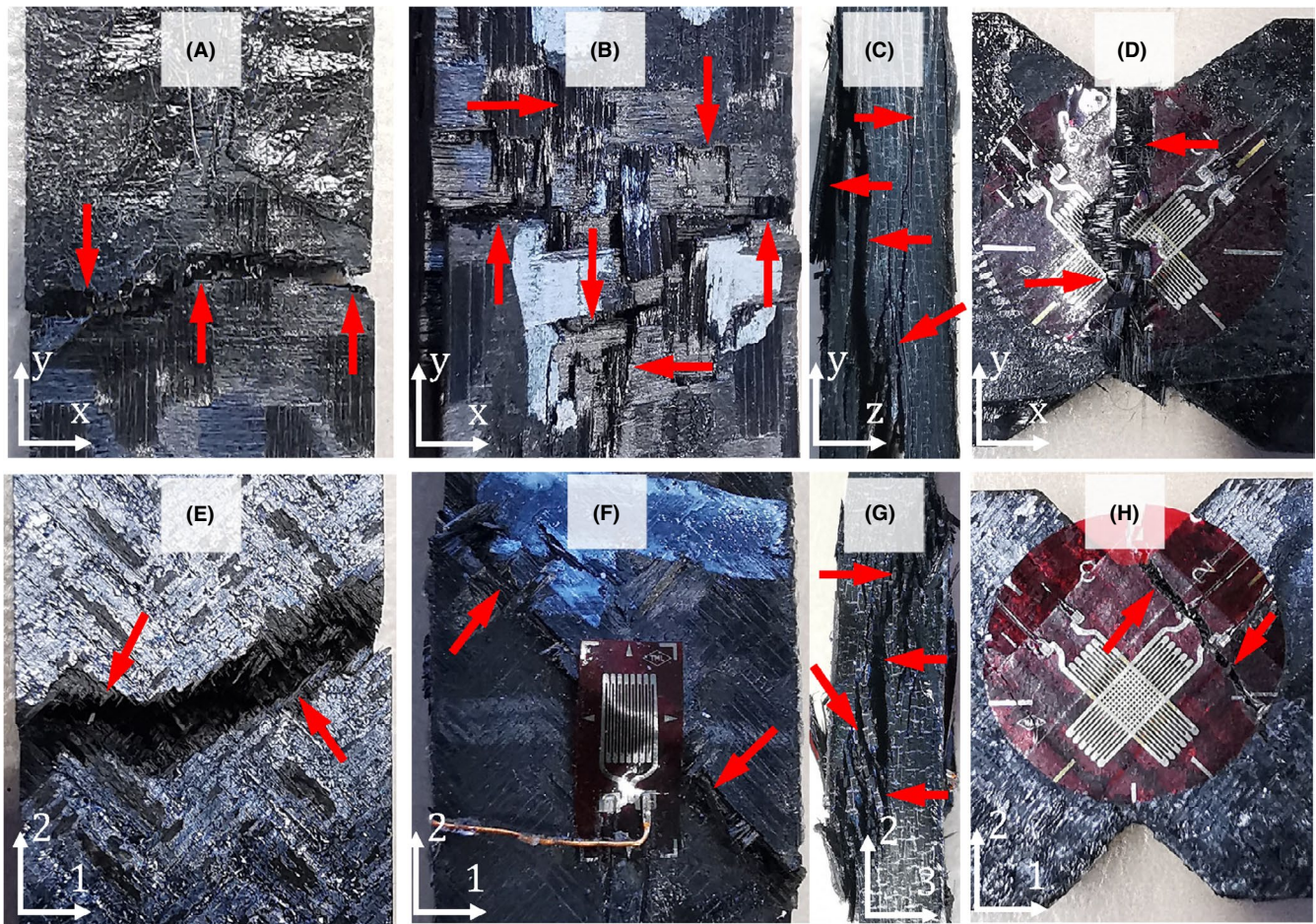| Failure properties						
	$\sigma_x^T = \sigma_y^T$ [MPa]	$\varepsilon_x^T = \varepsilon_y^T$ [%]	$\sigma_x^C = \sigma_y^C$ [MPa]	$\varepsilon_x^C = \varepsilon_y^C$ [%]	τ_{xy} [MPa]	γ_{xy} [%]
0° & 90°	125.7 ± 13.1	0.25 ± 0.03	329.9 ± 15.4	—	71.7 ± 0.9	3.09 ± 0.13
	$\sigma_1^T = \sigma_2^T$ [MPa]	$\varepsilon_1^T = \varepsilon_2^T$ [%]	$\sigma_1^C = \sigma_2^C$ [MPa]	$\varepsilon_1^C = \varepsilon_2^C$ [%]	τ_{12} [MPa]	γ_{12} [%]
+45° & −45°	95.0 ± 1.4	1.15 ± 0.04	135.7 ± 4.1	1.29 ± 0.16	126.5 ± 5.9	0.33 ± 0.02

FIGURE 4 Failure paths (red arrows) of tested C/C-SiC samples with fiber orientation 0° & 90° (with x–y axis and z-axis is for thickness direction) and +45° & −45° (with 1–2 axis and 3-axis is for thickness direction), A) 0° & 90° uniaxial tension; B) and C) 0° & 90° uniaxial compression; D) 0° & 90° Iosipescu-shear; E) +45° & −45° uniaxial tension; F) and G) +45° & −45° uniaxial compression; H) +45° & −45° Iosipescu-shear

A 0° & 90° specimen failed under uniaxial compression is shown in Figure 4B. Over the fracture area, it can be observed that a lot of fiber bundles are sticking out of the plane, leaving a rather rough and uneven appearance on the specimen surface, which is typical in compressive failure due to the typical kink band failure mechanism for fibers lying in the loading direction and transverse crushing for the tows perpendicular to the loading direction. The observed out-of-plane deformation in this case was exacerbated by the undulations in the fabric preform and the delaminations initiated from the edges of the specimen prior to the catastrophic fracture as shown in Figure 4C.

The Iosipescu-shear failure mode of a 0° & 90° specimen is shown in Figure 4D. The fracture is right across the specimen over the cross-section where reasonably pure shear was expected. It runs along the direction of one of the arrays of fibers and perpendicular to the other array. The failure was due to the relative sliding of the opposite halves of the specimen along the fracture. As a result, the fracture area is not as neat as that due to tension but much tidier than that due to compression.

The failure modes of the +45° & −45° specimens due to uniaxial tension and compression are shown in Figure 4E and Figure 4F, respectively. Both exhibit a 45° characteristic, that is, the fracture is along the fiber direction of one of the arrays of the fiber tows and perpendicular to the other array. A clear difference can be identified in terms of the neatness of the fracture, the former is clean leaving a smooth specimen surface behind, while the latter tends to leave a slightly rougher fracture area due to the sliding tendency. Another subtle difference is the fracture in the former case shows a degree of zig-zag appearance whilst the latter tends to show as a straight line. The presence of tension along with the dominating shear over the fracture surface allows the fracture to take place wherever the critical condition was met. However, when the dominating shear is accompanied with compression across the fracture surface, the sliding tendency would be retarded if the fracture surface had not been lined up properly. The surface roughness of the specimen failed under compression is more pronounced around the edge of the specimen due to the premature delaminations as shown in Figure 4G.

The Iosipescu-shear failure mode of a +45° & −45° specimen is shown in Figure 4H. The fracture is not within the zone where pure shear was expected and it probably would never be contained within this zone, given the specimen set up. The fracture initiated at the notch and propagated along the direction of array fiber tows perpendicular to the local tensile stress. The fracture bears similarity to the tensile fracture in the 0° & 90° specimen as shown in Figure 4A. It did not seem to have been influenced by the presence of the compressive stress in the direction parallel to the fracture surface.

4.2 | Theoretical predictions of elastic properties and failure

The C/C-SiC laminates produced according to the process as described in Section 0 will be considered as an orthotropic material without involving any microscopic details. It is assumed that any effects of the microscopic details have been reflected through the effective elastic and strength properties of the composite. There are two sets of independent principal axes, 45° apart as shown in Figure 2. The elastic and strength properties of the material have been measured independently in these two sets of principal coordinate systems. The properties measured in x–y coordinate system (0°–90°) will be

employed as the input data for the predictions of the deformation and failure of the material when it is loaded in uniaxial tension and compression and pure shear in the 1–2 coordinate system (±45°), which are all combined stress states in the x–y coordinate system. The experimental data measured in the 1–2 system (Table 2) maintain their complete independence from the predictions. The predicted deformation and failure will be compared with the experimental data as valid means of verifications of the analysis.

4.2.1 | Prediction of stress-strain relationships

Stresses between the two sets of principal coordinate systems are interrelated through the conventional coordinate transformation as listed in Table 3, where σ^* and τ^* are the magnitudes of loading in uniaxial and pure shear cases, ε^* and γ^* are the magnitudes of the applied strains in uniaxial and pure shear stress states, and v_{xy} is the Poisson' ratio of the material in the x–y axes. While the stress states in the loading coordinate system are either uniaxial or pure shear, they correspond to a combined stress state in the other coordinate system in which the material also remains orthotropic. It should be pointed out that under a uniaxial stress state, the corresponding strain state is not at all uniaxial due to the Poisson's effect,

TABLE 3 Stresses and strains under testing conditions (black) and their transformations to the other principal coordinate systems (red)

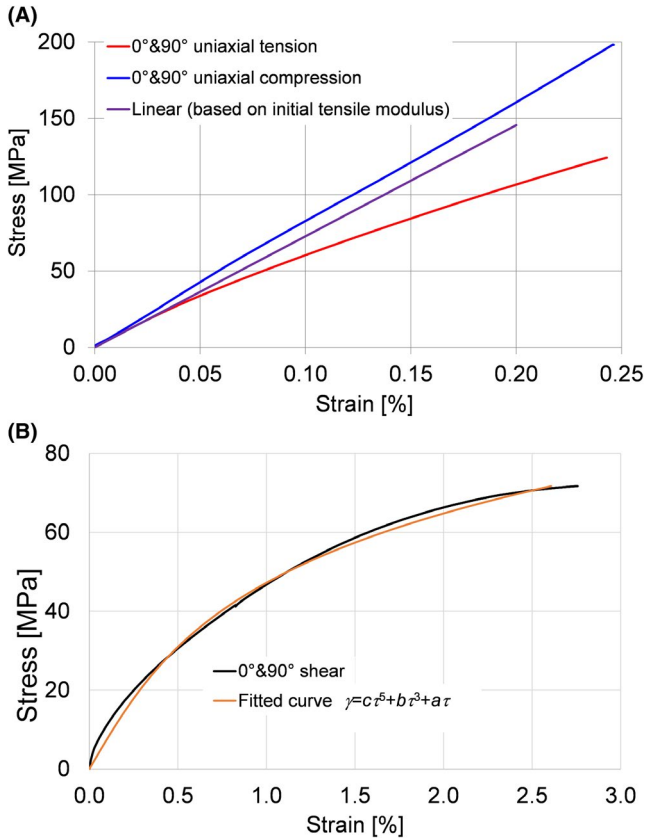|	**Stresses**		**Strains**	
Coordinate system	**x–y**	**1–2**	**x–y**	**1–2**
Uniaxial tension along x-axis	$\sigma_x = \sigma^*$ $\sigma_y = 0$ $\tau_{xy} = 0$	$\sigma_1 = \sigma^*/2$ $\sigma_2 = \sigma^*/2$ $\tau_{12} = -\sigma^*/2$	$\varepsilon_x = \varepsilon^*$ $\varepsilon_y = -v_{xy}\varepsilon^*$ $\gamma_{xy} = 0$	$\varepsilon_1 = \varepsilon_2 = \dfrac{\varepsilon^*\left(1-v_{xy}\right)}{2}$ $\gamma_{12} = -\varepsilon^*\left(1+v_{xy}\right)$
Uniaxial compression along x-axis	$\sigma_x = -\sigma^*$ $\sigma_y = 0$ $\tau_{xy} = 0$	$\sigma_1 = -\sigma^*/2$ $\sigma_2 = -\sigma^*/2$ $\tau_{12} = \sigma^*/2$	$\varepsilon_x = -\varepsilon^*$ $\varepsilon_y = v_{xy}\varepsilon^*$ $\gamma_{xy} = 0$	$\varepsilon_1 = \varepsilon_2 = -\dfrac{\varepsilon^*\left(1-v_{xy}\right)}{2}$ $\gamma_{12} = \varepsilon^*\left(1+v_{xy}\right)$
Pure shear in x–y-axes	$\sigma_x = 0$ $\sigma_y = 0$ $\tau_{xy} = \tau^*$	$\sigma_1 = \tau^*$ $\sigma_2 = -\tau^*$ $\tau_{12} = 0$	$\varepsilon_x = 0$ $\varepsilon_y = 0$ $\gamma_{xy} = \gamma^*$	$\varepsilon_1 = \gamma^*/2$ $\varepsilon_2 = -\gamma^*/2$ $\gamma_{12} = 0$
Uniaxial tension along 1-axis	$\sigma_x = \sigma^*/2$ $\sigma_y = \sigma^*/2$ $\tau_{xy} = -\sigma^*/2$	$\sigma_1 = \sigma^*$ $\sigma_2 = 0$ $\tau_{12} = 0$	$\varepsilon_x = \varepsilon_y = \dfrac{\varepsilon^*\left(1-v_{12}\right)}{2}$ $\gamma_{xy} = -\varepsilon^*\left(1+v_{12}\right)$	$\varepsilon_1 = \varepsilon^*$ $\varepsilon_2 = -v_{12}\varepsilon^*$ $\gamma_{12} = 0$
Uniaxial compression along 1-axis	$\sigma_x = -\sigma^*/2$ $\sigma_y = -\sigma^*/2$ $\tau_{xy} = \sigma^*/2$	$\sigma_1 = -\sigma^*$ $\sigma_2 = 0$ $\tau_{12} = 0$	$\varepsilon_x = \varepsilon_y = -\dfrac{\varepsilon^*\left(1-v_{12}\right)}{2}$ $\gamma_{xy} = \varepsilon^*\left(1+v_{12}\right)$	$\varepsilon_1 = -\varepsilon^*$ $\varepsilon_2 = v_{12}\varepsilon^*$ $\gamma_{12} = 0$
Pure shear in 1–2-axes	$\sigma_x = \tau^*$ $\sigma_y = -\tau^*$ $\tau_{xy} = 0$	$\sigma_1 = 0$ $\sigma_2 = 0$ $\tau_{12} = \tau^*$	$\varepsilon_x = \gamma^*/2$ $\varepsilon_y = -\gamma^*/2$ $\gamma_{xy} = 0$	$\varepsilon_1 = 0$ $\varepsilon_2 = 0$ $\gamma_{12} = \gamma^*$

(A)

(B)

FIGURE 5 Stress-strain curves in x–y axes and their approximations: (A) uniaxial tension and compression and linear approximation based on the tensile modulus; (B) shear stress-strain curve and its polynomial fit

although a pure shear stress state results in a pure shear strain state. The combined stresses and strains in the other coordinate system as shown in Table 3 are obtained exclusively through coordinate transformations as a consequence of the fact that stresses and strains are all components of tensors. They are always applicable whether the material behaves linearly or nonlinearly in terms of its stress-strain relationship, understanding that the Poisson's ratio v_{xy} may not necessarily be a constant in a generally nonlinear case.

There has not been a systematic and practical theoretical framework to describe the nonlinear stress-strain relationship fully in general, let alone for ceramic matrix composites (CMCs) as a relatively new type of composites. However, if the stress-strain relationship under uniaxial tension and uniaxial compression in the 0° and 90° directions can be approximated as linear with the common Young's modulus as obtained under tension, and the nonlinearity is only present in the in-plane shear in the x–y axes, then the uniaxial tension and compression and pure shear in the 1–2 axes can be obtained theoretically.[31] This is one for the areas where a novel contribution has been made in this paper for the composite concerned.

A marginal difference was reported in Ref [10] between the tensile and compressive Young's moduli. If there was

a genuine disparity, the material would have to be considered bimodulus, which would be a significant source of nonlinearity. However, the difference reported in Ref [10] as quoted in Table 2 is believed to be caused by the lack of waisted gauge length in the samples employed for the compression tests, therefore, the uniaxial stress state was not observed during the test. This has been validated by the authors through conducting independent compression tests using C/C-SiC specimens of a dumbbell shape, same as was employed in tensile tests (tensile sample in Table 1), while keeping the load level sufficiently low to avoid undue buckling. The measured Young's modulus under compression was then hardly any different from that obtained under tension (Table 2). This justifies the use of tensile Young's modulus (E^T) for both tension and compression. Such a linear approximation is compared with the experimentally obtained stress-strain curves in tension and compression for orientation 0° & 90° (absolute values) in Figure 5A. The linear approximation will be employed in the subsequent analyses as the input data.

A rational account on the nonlinearity in in-plane shear can be found in Ref [31] although it was formulated for transversely isotropic materials under 3D stress states. The outcome is applied to the current problem of an orthotropic material but under a plane stress condition. The fitted polynomial to the 5th order as shown in Figure 5B can be used as a reasonable approximating whilst maintaining the consistency in the theoretical framework for the analysis.

Transforming stresses from 1–2 coordinate system to x–y system, one obtains

$$\sigma_x = \frac{1}{2}(\sigma_1 + \sigma_2) - \tau_{12}$$
$$\sigma_y = \frac{1}{2}(\sigma_1 + \sigma_2) + \tau_{12} \qquad (1)$$
$$\tau_{xy} = \frac{1}{2}(\sigma_1 - \sigma_2)$$

In the x–y coordinate system, strains are related to stresses as follows:

$$\varepsilon_x = \frac{\sigma_x}{E_x} - \frac{v_{xy}\sigma_y}{E_x}$$
$$\varepsilon_y = -\frac{v_{xy}\sigma_x}{E_x} + \frac{\sigma_y}{E_y} \qquad (2)$$
$$\gamma_{xy} = a\tau_{xy} + b\tau_{xy}^3 + c\tau_{xy}^5$$

where from the curve-fitting as shown in Figure 5B, $a = 0.013\,\text{MPa}^{-1}$, $b = 3.0 \times 10^{-6}\,\text{MPa}^{-3}$ and $c = 3.0 \times 10^{-10}\,\text{MPa}^{-5}$ with the shear strain being in percentage.

Making use of the stress transformation above, strains in the x–y system can be expressed in terms of stresses in the 1–2 system. Substituting the obtained relationship into the following strain transformation formulae:

$$\varepsilon_1 = \frac{1}{2}\left(\varepsilon_x + \varepsilon_y\right) + \frac{1}{2}\gamma_{xy}$$

$$\varepsilon_2 = \frac{1}{2}\left(\varepsilon_x + \varepsilon_y\right) - \frac{1}{2}\gamma_{xy} \tag{3}$$

$$\gamma_{12} = -\left(\varepsilon_x - \varepsilon_y\right)$$

one can relate the strains in 1–2 system to the stresses in the same coordinate system as follows, given that $E_y = E_x$,

$$\varepsilon_1 = \frac{1}{4}\left(\sigma_1 - \sigma_2\right)\left(\frac{2}{E_x}\left(1 - v_{xy}\right) + a + \frac{1}{4}b\left(\sigma_1 - \sigma_2\right)^2 + \frac{1}{16}c\left(\sigma_1 - \sigma_2\right)^4\right)$$

$$\varepsilon_2 = \frac{1}{4}\left(\sigma_1 - \sigma_2\right)\left(\frac{2}{E_x}\left(1 - v_{xy}\right) - a - \frac{1}{4}b\left(\sigma_1 - \sigma_2\right)^2 - \frac{1}{16}c\left(\sigma_1 - \sigma_2\right)^4\right) \tag{4}$$

$$\gamma_{12} = \frac{2\left(1 + v_{xy}\right)}{E_x}\tau_{12}$$

Under uniaxial stress (tension or compression) in 1-direction and pure shear in 1–2 system as special cases, the strains in the 1–2 coordinate system can be found respectively as follows:

$$\varepsilon_1 = \frac{\sigma_1}{4}\left(\frac{2\left(1 - v_{xy}\right)}{E_x} + a + \frac{1}{4}b\sigma_1^2 + \frac{1}{16}c\sigma_1^4\right)$$

$$\varepsilon_2 = \frac{\sigma_1}{4}\left(\frac{2\left(1 - v_{xy}\right)}{E_x} - a - \frac{1}{4}b\sigma_1^2 - \frac{1}{16}c\sigma_1^4\right) \tag{5}$$

$$\gamma_{12} = 0$$

and

$$\varepsilon_1 = 0$$

$$\varepsilon_2 = 0$$

$$\gamma_{12} = \frac{2\left(1 + v_{xy}\right)}{E_x}\tau_{12} \tag{6}$$

Using the above, the stress-strain curves in the 1–2 system can be predicted as shown in Figure 6, where uniaxial tension and compression coincide with each other because the tensile Young's modulus was employed for both tension and compression as was explained earlier.

The four independent elastic constants (E^T, E^C, G, and γ) of C/C-SiC for fiber orientation +45° & −45° were evaluated based on the input from 0°&90° tests. The calculated results are compared with the experimental values (Table 2) in Figure 7 and a relatively good agreement can be observed.

Since the Young's modulus employed as the input was from the tensile test obtained in the x–y system (0°–90°), one might expect the predicted stress-strain curve to be closer to the tensile one in the 1–2 system (±45°), as opposed to what is shown in Figure 6A. The disparity there is because of the slight nonlinearity present in the tensile stress-strain curve in the x–y system as shown in Figure 5A, which has been
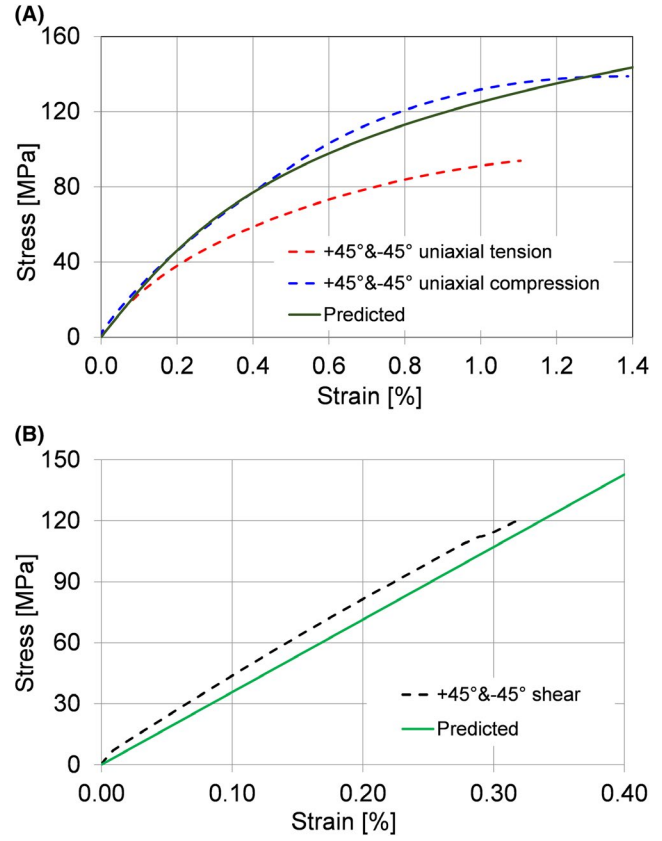

FIGURE 6 Predicted stress-strain curves in the 1–2 coordinate system and compared with experimental data: (A) uniaxial tension and compression; (B) pure shear
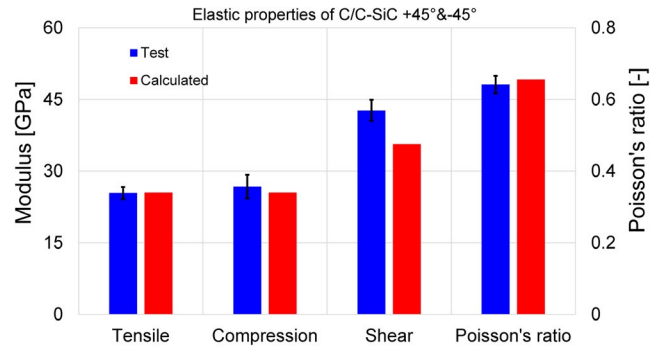

FIGURE 7 Comparison of calculated elastic properties to test results of C/C-SiC with fiber orientation of +45° & −45° under uniaxial tensile, compression, and pure shear loads

neglected in the above prediction as explained above, rendering an overestimation of the stiffness at increased strain levels. Apart from this, the predicted stress-strain curves in the 1–2 coordinate system as shown in Figure 6 are reasonably accurate, allowing unavoidable experimental errors.

One might imagine that the process could be reversed, that is, the stress-strain curves under uniaxial tension and

compression and pure shear in the x–y coordinate system ($0°$–$90°$) could be predicted from those in the 1–2 system ($\pm 45°$). However, this is not possible as there has not been a practical and rational theoretical framework to support the characterization of a generally nonlinear material, as mentioned before. There is not a rational formulation of nonlinear stress-strain relationship under direct stresses, such as that exhibited by for the $+45°$ & $-45°$ specimens as shown in Figure 3. As an illustration, the first two equations in (2) are formulated based on the superposition law which does not applied in nonlinear problems in general. A practical consideration is that there has been no explicit guideline specifying the exact number of elastic constants required and the experimental means to measure them.

4.2.2 | Predictions of failure

Material testing has been conducted under uniaxial tension and compression and pure shear in each of the two principal coordinate systems (section 0). The set of elastic and strength properties from each coordinate system (Table 2) will be employed to facilitate the failure predictions under arbitrary stress states in the respective coordinate system. Once the uniaxial tension, compression and pure shear states in the 1–2 coordinate system are expressed in the x–y system, they are combined stress states. Failure criteria can be applied to these combined stress states and predictions of failure can be made based on the strength properties measured in the x–y coordinate system ($0°$–$90°$). These predictions can then be compared with experimentally measured strengths in the 1–2 system ($\pm 45°$), which will serve as independent verifications for the failure predictions.

It should be emphasized that the measured strengths in the 1–2 system are valid materials properties because the material in the 1–2 coordinate system is orthotropic, the testing and measurement methods are therefore properly supported by available industrial standards (Table 1). In any coordinate system other than x–y and 1–2, the material will not demonstrate its orthotropy. There is no industrial standard supporting tests conducted in such a coordinate system yet. Therefore, the validity of experimental data measured in off-axis directions other than $\pm 45°$, such as $+30°/-60°$ or $+15°/-75°$ as presented in Ref [11] should be not be taken for granted, because such directions are not in material's principal axes and direct stresses tend to induce shear strains whilst the testing fixture does not allow free shear deformation. As a result, a degree of shear force is applied which causes sideways bending, compromising the uniformity of applied uniaxial stress condition.

The failure of the material under uniaxial tension and compression and pure shear in the 1–2 coordinate system will be predicted. The problem however will be formulated

in the x–y coordinate system in which the strength properties are measured. In the x–y coordinate system, the uniaxial tension and compression and pure shear in the 1–2 system will be combined stress states as given in Table 3 already. As the material is not transversely isotropic, those failure criteria only applicable to transversely isotropic materials will not be relevant here. In this work, three different failure criteria, which are not explicitly restricted to transversely isotropic materials, have been selected. They are the maximum stress criterion and Tsai-Wu criterion, which are stress-based composite failure criteria, and the maximum strain criterion which is a strain-based criterion, expressed as follows.

The maximum stress criterion:

$$\frac{\sigma_i}{\sigma_i^T} \leq 1 \text{ if } \sigma_i \geq 0 \text{ or } \frac{|\sigma_i|}{\sigma_i^C} \leq 1 \text{ if } \sigma_i < 0, \quad (i = x, y) \quad (7)$$

$$\frac{|\tau_{xy}|}{\tau_{xy}^F} \leq 1. \quad (8)$$

The Tsai-Wu criterion:

$$\left(\frac{1}{\sigma_x^T} - \frac{1}{\sigma_x^C} \right) \sigma_x + \left(\frac{1}{\sigma_y^T} - \frac{1}{\sigma_y^C} \right) \sigma_y + \frac{1}{\sigma_x^T \sigma_x^C} \sigma_x^2$$
$$+ \frac{1}{\sigma_y^T \sigma_y^C} \sigma_y^2 - \frac{1}{\sqrt{\sigma_x^T \sigma_x^C \sigma_y^T \sigma_y^C}} \sigma_x \sigma_y + \frac{1}{\left(\tau_{xy}^F \right)^2} \tau_{xy}^2 \leq 1, \quad (9)$$

The maximum strain criterion:

$$\frac{\varepsilon_i}{\varepsilon_i^T} \leq 1 \quad \text{if} \quad \varepsilon_i \geq 0 \quad \text{or} \quad \frac{|\varepsilon_i|}{\varepsilon_i^C} \leq 1 \quad \text{if} \quad \varepsilon_i < 0 \quad (i = x, y), \quad (10)$$

$$\frac{|\gamma_{xy}|}{\gamma_{xy}^F} \leq 1. \quad (11)$$

All above criteria are based on macroscopic behavior of the composite. Micro-mechanical models are available in the literature, for example,[33-35] from which more extensive list of publications in this filed can be found, but for failure predictions they are some distance from maturity. A typical difficulty associated with micro-mechanical models is the lack of required material properties and other parameters at the corresponding length scale. There is no standard testing method to measure them, either. The composite concerned in this paper is made from woven fabric the geometry of which at meso-scale is complicated where an accurate description is not available in general. To facilitate such models, assumed values are often

employed, undermining the predictiveness of these models. The Tsai-Wu criterion is a relatively more established theory, although one outstanding issue of it did not get resolved until fairly recently after some rational considerations made to it.[27] The composite is a genuinely orthotropic material as its macroscopic scale, but the rationalization made to the Tsai-Wu criterion in Ref. [27] was limited to transversely isotropic materials. There has been no rational way to determine some of the coefficients involved in the criterion for genuinely orthotropic materials. The authors are intrigued to put the criterion to test against a material which is genuinely orthotropic whilst the basic strength properties are available, so that an objective assessment of the criterion can be made. This would motivate further attempt to rationalize the Tsai-Wu criterion for genuinely orthotropic materials, although this is obviously beyond the scope of the present paper.

Their suitability of the criteria as expressed in Equations 7–11 will be tested by applying them to the material concerned here (C/C-SiC), for which a reasonably complete set of strength properties are available, and verifications can be made against tests conducted under the respective uniaxial tension, compression and pure shear. Furthermore, the failure modes are predicted through the maximum stress and maximum strain criterion, and the outcomes are presented in Table 4.

Due to the fact that several strain gauges on the 0° & 90° specimens for the uniaxial compression tests had failed before the failure of samples, the ultimate strain was not specified in Tables 2 and 4. However, on the assumption that the stress-strain behavior of fiber orientation 0°&90° is linear under compression loading (Figure 3), the maximum strain value is calculated from compression strength and modulus to be approximately 0.45%. The predicted strength (through maximum stress and Tsai-Wu criterion) and failure strain values (through maximum strain criterion) from Table 4 are compared with the test results in Table 2 and are shown in Figure 8A,B for fiber orientation +45° & −45° and 0° & 90°, respectively.

The following observations can be made on the predicted strength and failure modes.

TABLE 4 Predicted and experimental strengths, strains and failure modes of C/C-SiC material with fibers orientated at +45° & −45° and 0° & 90°. The data in brackets are the absolute value of difference between experimental and predicted result. Generic failure modes obtained under uniaxial or pure shear stress states in the directions of fiber tows are highlighted in red

Predicted failure of +45°&−45° specimens loaded in 1- and 2-axes using the strengths in 0° & 90° directions in x- and y-axes			
	Max stress criterion	**Tsai-Wu criterion**	**Max strain criterion**	**Experiment Strength / failure strain**
Uniaxial tension	143.4 MPa (48.4 MPa)	97.5 MPa (2.5 MPa)	0.51% (0.64%)	95 MPa /1.15%
	Shear mode in 0°−90° directions	—	Tensile mode in 0°−90° directions	Shear mode in 0°−90° directions
Uniaxial compression	143.4 MPa (7.7 MPa)	187.6 MPa (51.9 MPa)	0.93% (0.36%)	135.7 MPa /1.29%
	Shear mode in 0°−90° directions	—	Compressive mode in 0°−90° directions	Shear mode in 0° or 90° direction
Pure shear	125.7 MPa (0.8 MPa)	117.6 MPa (8.9 MPa)	0.50% (0.17%)	126.5 MPa /0.33%
	Tensile mode in 0° or 90° direction	—	Tensile mode in 0°−90° directions	Tensile mode in 0° or 90° direction

Predicted failure of 0° & 90° specimens loaded in x- and y-axes using the strengths in +45° & −45° directions in 1- and 2-axes			
	Max stress criterion	**Tsai-Wu criterion**	**Max strain criterion**	**Experiment Strength / failure strain**
Uniaxial tension	190.0 MPa (64.3 MPa)	129.8 MPa (4.1 MPa)	0.21% (0.04%)	125.7 MPa /0.25%
	Tensile mode in ±45° directions	—	Shear mode in ±45° directions	Tensile mode in 0°−90° directions
Uniaxial compression	253.0 MPa (76.9 MPa)	220.0 MPa (109.9 MPa)	0.21%	329.9 MPa /-
	Shear mode in ±45° directions	—	Shear mode in ±45° directions	Compressive mode in 0°−90° directions
Pure shear	95.0 MPa (23.3 MPa)	65.6 MPa (6.1 MPa)	2.30% (0.79%)	71.7 MPa /3.09%
	Tensile mode in ±45° directions	—	Tensile mode in ±45° directions	Shear mode in 0°−90° directions

The data in brackets are the absolute value of difference between experimental and predicted result. Generic failure modes obtained under uniaxial or pure shear stress states in the directions of fiber tows are highlighted in red.
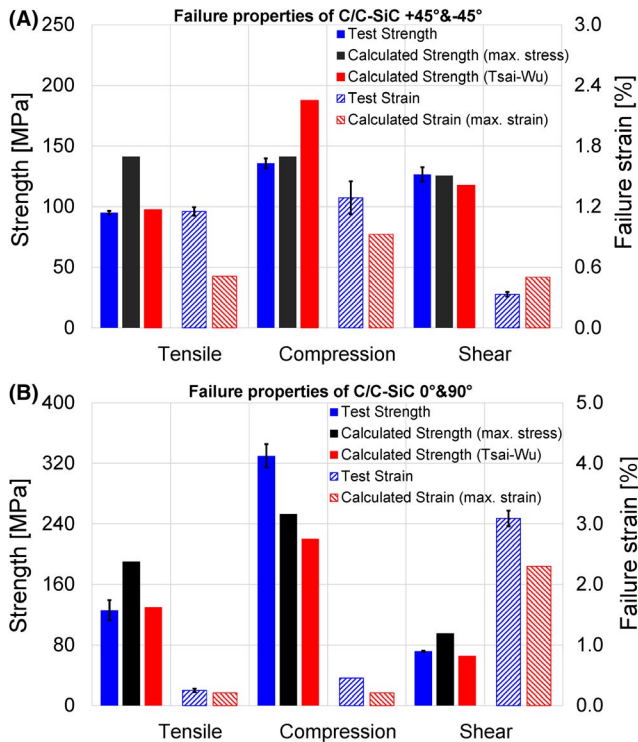
FIGURE 8 Comparison of calculated failure properties to test results of C/C-SiC under tensile, compression, and shear loads with fiber orientation of (A) +45° & −45° and (B) 0° & 90°

The maximum stress criterion:

1. Under uniaxial tension in the 1–2 system (±45°), the maximum stress criterion overestimates the strength significantly (Figure 8A). However, given the dominance of the predicted stress ratios corresponding to the tensile mode and shear mode, a reasonably high level of confidence can be placed on the predicted failure mode which is shear along the direction of one of the arrays of fibers while perpendicular to the other array, which agrees with the failure mode as observed in the tested C/C-SiC with orientation of +45° & −45° in Figure 4E.

2. A rather close prediction of the compression strength (Figure 8A) has been achieved and the failure mode should be along the direction of one of the arrays of fibers whilst perpendicular to the other array, but in the presence of compression transverse to the fibers, which again agree well with the failure mode as shown in Figure 4F. However, the agreement in the strength should not be taken literally and the predicted failure here might not be what was actually observed in experiments. In the actual experiment, substantial delaminations took place around the edges of the specimen under loading (Figure 4G). The observed failure was likely the consequence of post-buckling deformation of delaminated plies, which was definitely a mode of premature failure, rather than the expected failure of the material under uniaxial

compression in the direction 1 or 2. A simple argument can be presented as follows. As the critical compressive stress level in directions along and transverse to fibers is so much higher than that for shear, the failure mode should be in shear beyond any doubt. The strength along fibers under pure shear is 71.7 MPa as measured in the x–y system. The shear component in the uniaxial compression in the 1–2 system is half of the magnitude of the applied load and therefore the load level corresponding to shear failure should be twice of the along fibers shear strength, that is, 143.4 MPa. The presence of transverse compression should enhance the shear strength, if it makes any difference. The theoretical compressive failure load level should be at least 143.4 MPa. However, the actual strength measured is only 135.7 MPa. Readers are further reminded that the uniaxial stress state can never be well-maintained in a compression test, given the testing conditions as defined in the standard, where the standard merely represents a compromise between ideal testing requirements and practicality. There is a good reason to challenge the truthfulness of the experimentally measured strength and the observed failure mode under this particular loading condition.

3. The shear strength has been accurately predicted. Again, the close agreement should not be taken for granted, as there is a noticeable margin between the ideal uniformity of the pure shear stress state and what could be achieved in the Iosipescu-shear test. The failure mode should almost certainly be tensile in direction of one of the arrays of fibers, with the other array of fibers in the perpendicular direction being under compression (Figure 4H).

The maximum strain criterion:

4. Predictions are generally unreliable and often in wrong failure modes. It should not be recommended for applications to genuine orthotropic materials, no matter how much one prefers strain-based criteria.

The Tsai-Wu criterion:

5. It tends to predict failure reasonably well with the largest discrepancy found for compressive failure prediction. However, as argued above, the measured compressive strength was significantly underestimated due to the limitations in experimentation, therefore, the applicability of the Tsai-Wu criterion to the compressive failure prediction should not be dismissed based on lack of close agreement with the experiment this case. No failure modes are predicted in the Tsai-Wu criterion.

Summarizing the above discussion, for genuine orthotropic materials, such as C/C-SiC considered in this paper, under the plane stress condition, the Tsai-Wu criterion seems to offer a reasonable prediction for the strengths. It can be assisted by

the maximum stress criterion to obtain an indicative prediction of the failure mode for the composite concerned. However, it should be pointed out that the prediction of failure mode is only meaningful when there is a clear dominance of a particular stress component. Otherwise, the failure mode may not be as obvious as one would wish. This might also undermine the justifications for any mode dependent failure criterion.

Purely from the perspective of the orthotropy, the coordinate systems x–y and 1–2 are equally useful, as both are principal systems. Practically, the differences should not be overlooked. In the discussion of stress-strain curves as in the previous subsection 0, predictions can be made one way but not the other, based on the existing development of nonlinear elasticity. For strength predictions, there is no restriction on the direction of the process, that is, predicting the strengths in the 1–2 system (±45°) based on those in the x–y system (0°–90°), as has been carried out in the top half of Table 4 and also discussed above, or predicting strength in the x–y system based on those in the 1–2 system. The reverse process has been carried out with the results included in the second half of Table 4. It can be seen that none of the failure modes predicted from this reversed process according to both the maximum stress and maximum strain criteria is relevant because one would expect the fracture surfaces aligned with 1 or 2 axis, that is, 45° from the fibers in the x–y plane. The predicted strengths are just as inaccurate as the failure modes predicted. One should be able to draw a clear conclusion here on the applicability of these two failure criteria. The maximum strain criterion is deemed to be inapplicable to genuine orthotropic materials and the maximum stress criterion is relevant in failure mode predictions, but predicted strengths could contain significant errors and the predictions are relevant only if the principal axes of the coordinate system happen to coincide with the directions of fibers. This has never been revealed previously.

Following the reversed process as described above, the Tsai-Wu criterion outperformed the other two. The predicted tensile and shear strengths are in fact a little too close to the experimental values to be true. These are of course accompanied by an excessively underestimated compressive strength. In absence of better failure criterion applicable to genuine orthotropic materials, the Tsai-Wu criterion might serve as an interim solution, if due care has been exercised with its accuracy justified with respect to that of its input data. It can be misleading if it is used as a black box. The state-of-the-art on composite failure criteria is simply not mature enough for any attempts of this kind.

5 | CONCLUSIONS

In this work, the mechanical behaviors, especially the failure properties, of LSI-based C/C-SiC were investigated and theoretical predictions of the elastic properties and failure were compared with the experimental data. The main conclusions of this work are as follows.

1. According to the lamination process of preform, the composite under investigation can be considered as an orthotropic material with two sets of independent principal axes, 0°–90° and ±45°. The mechanical characteristics, including elastic constants, stress-strain behaviors, and failure properties were investigated independently in these two principal coordinate systems under uniaxial tension, compression, and pure shear loads. The different failure modes of tested samples were analyzed and served as indication to evaluate the accuracy of predicted results.

2. The properties measured in x–y coordinate system (0°–90°) were employed as the input data for the modeling of the elastic constants and deformations in the 1–2 coordinate system (±45°) under uniaxial tension, compression, and pure shear loadings, in which the stress states are combined whilst the material remains orthotropic. The stresses between the two sets of principal coordinate systems are interrelated through the conventional coordinate transformation. The predicted four independent elastic constants (E^T, E^C, G, and γ) and stress-strain curves with fiber orientations at +45° & −45° show good agreement to the experimental results. However, a reversed process for the prediction of same values in the x–y coordinate system (0°–90°) from the data obtained in the 1–2 system (±45°) as the input is not possible, because no practical or rational theoretical framework can support the characterization of a generally nonlinear material, as is the case fiber orientations at +45° & −45° under uniaxial tension and compression.

3. Based on the strength properties measured in the x–y coordinate system (0°–90°), the maximum stress, Tsai-Wu and maximum strain criteria have been applied for the prediction of failure properties in the 1–2 direction (±45°). In comparison with the other two criteria, the calculated strengths through Tsai-Wu criterion are in good agreement with experimental values except the case under uniaxial compression load, where the experimental strength corresponded to a premature failure mode. Furthermore, though the predicted strengths are not accurate, the maximum stress criterion could offer indicative prediction of the failure mode, if there is a significant dominance of a stress component. The predictions of failure strains as well as associated failure modes through maximum strain criterion were found to be generally unreliable and this criterion is therefore not be recommended for applications to genuine orthotropic CMCs.

The failure properties of the C/C-SiC composite have been measured in two sets of principal coordinate systems

and applied to three different failure criteria for the evaluation of the applicability of each of them. The same approach can be extended into other CMCs of genuine orthotropic characteristics. This will be of a significant value in the design and development of CMC structures to meet stiffness, strength and failure strain requirements in new application fields.

ACKNOWLEDGMENT

ORCID

Yuan Shi https://orcid.org/0000-0002-4210-9069

REFERENCES

1. Kochendörfer R, Lützenburger N, editors. Applications of CMCs Made via the Liquid Silicon Infiltration (LSI) Technique. 4th International Conference on High Temperature Ceramic Matrix Composites (HT-CMC 4); 2001; Munich, Germany.
2. Krenkel W, Heidenreich B, Renz R. C/C-SiC composites for advanced friction systems. Adv Eng Mater. 2002;4(7):427–36.
3. Krenkel W, Berndt F. C/C–SiC composites for space applications and advanced friction systems. Mater Sci Eng, A. 2005;412(1–2):177–81.
4. Frieß M, Krenkel W, Kochendörfer R, Brandt R, Neuer G, Maier H-P. Ceramic matrix composites – the Key Materials for re-entry from space to earth. In: Jacob D, Sashs G, Wagner S, editors. Basic research and technologies for two-stage-toorbit vehicles. Weinheim: Wiley-VCH; 2005. p. 499–526.
5. Heidenreich B. Manufacture and applications of C/C-SiC and C/SiC composites. In: Singh JP, Bansal NP, Goto T, Lamon J, Choi SR, Mahmoud MM, Link G, et al., editors. Processing and properties of advanced ceramics and composites IV. Ceramic Transactions Series. Hoboken: John Wiley & Sons, Inc.; 2012. p. 183–98.
6. Ding W, Shi Y, Kessel F, Koch D, Bauer T. Characterization of corrosion resistance of C/C–SiC composite in molten chloride mixture MgCl2/NaCl/KCl at 700°C. npj Mater Degradation. 2019;3(1):1–9.
7. Stahl V, Shi Y, Kraft W, Lanz T, Vetter P, Jemmali R, et al. C/C-SiC component for metallic phase change materials. Int J Appl Ceram Technol. 2020;17(5):2040–50.
8. Shi Y, Dileep PK, Heidenreich B, Koch D. Determination and modeling of bending properties for continuous fiber reinforced C/C-SiC sandwich structure with grid core. Compos Struct. 2018;204:198–206.
9. Krenkel W. Development of a cost efficient process for the manufacture of CMC components. Doctoral Thesis, University of Stuttgart; 2000.
10. Shi Y, Kessel F, Friess M, Jain N, Tushtev K. Characterization and modeling of tensile properties of continuous fiber reinforced C/C-SiC composite at high temperatures. J Eur Ceram Soc. 2020;41(5):3061–71.

11. Hofmann S, Öztürk B, Koch D, Voggenreiter H. Experimental and numerical evaluation of bending and tensile behaviour of carbon-fibre reinforced SiC. Compos A Appl Sci Manuf. 2012;43(11):1877–85.
12. Breede F, Koch D, Maillet E, Morscher GN. Modal acoustic emission of damage accumulation in C/C–SiC composites with different fiber architectures. Ceram Int. 2015;41(9):12087–98.
13. Shi Y, Xiu Y, Koch D. Investigation of statistical distribution of C/C-SiC composite's mechanical properties. Key Eng Mater. 2019;809:131–9.
14. Hofmann S. Effect of interlaminar defects on the mechanical behaviour of carbon fibre reinforced silicon carbide. Stuttgart, Germany: University Stuttgart; 2013.
15. Breede F, Hofmann S, Jain N, Jemmali R. Design, manufacture, and characterization of a carbon fiber-reinforced silicon carbide nozzle extension. Int J Appl Ceram Technol. 2016;13(1):3–16.
16. Yang C, Jiao G, Guo H. Failure criteria for C/SiC composites under plane stress state. Theor Appl Mechanics Lett. 2014;4(2):021007.
17. Jain N, Koch D. Prediction of failure in ceramic matrix composites using damage-based failure criterion. J Composites Sci. 2020;4(4):183.
18. Chen Y, Shi Y, Chateau C, Marrow J. In situ X-ray tomography characterisation of 3D deformation of C/C-SiC composites loaded under tension. Compos A Appl Sci Manuf. 2021;145:106390.
19. Hinton MJ, Soden PD, Kaddour AS. Failure criteria in fibre-reinforced-polymer composites. Composites Sci Technol Part A, 1998, 58(7); Part B, 2002, 62(12-13) and Part C, 2004, 64(3-4).
20. Kaddour AS, Hinton MJ. Evaluation of theories for predicting failure in polymer composite laminates under 3-D states of stress. J Composite Mater. Part A, 2012, 46(19-20) and Part B, 2013, 47(6-7).
21. Kaddour AS, Hinton MJ, Smith PA, Li S. Benchmarking of matrix cracking, damage and failure models for composites: comparison between theories. J Compos Mater. 2013;47(20–21).
22. Li S, Sitnikova E. A critical review on the rationality of popular failure criteria for composites. Composites Commun. 2018;8:7–13.
23. Li S. The maximum stress failure criterion and the maximum strain failure criterion: their unification and rationalization. J Composites Sc. 2020;4(4):157.
24. Timoshenko SP. History of strength of materials. New York, NY: Dover Publications; 1983.
25. Tsai SW, Wu EM. A general theory of strength for anisotropic materials. J Compos Mater. 1971;5(1):58–80.
26. Tsai SW, Hahn HT. Introduction to composite materials. Boca Raton: Technomic Publishing Company, Inc.; 1980.
27. Li S, Sitnikova E, Liang Y, Kaddour A-S. The Tsai-Wu failure criterion rationalised in the context of UD composites. Compos A Appl Sci Manuf. 2017;102:207–17.
28. Hoffman O. The brittle strength of orthotropic materials. J Compos Mater. 1967;1(2):200–6.
29. DIN EN 1389: Advanced technical ceramics - Ceramic composites - Physical properties - Determination of density and apparent porosity. 2004.
30. Li S, Sitnikova E. Chapter 3 Material categorization and material characterization and Chapter 12 Applications to textile composites. Representative Volume Elements and Unit Cells- Concepts, Theory, Applications and Implementation. Duxford, UK: Woodhead Publishing Series in Composites Science and Engineering. Elsevier; 2020.

31. Li S, Xu M, Yan S, Sitnikova E. On the objectivity of the nonlinear along-fibre shear stress–strain relationship for unidirectionally fibre-reinforced composites. J Eng Math. 2021;127(1):1–13.

32. Shi Y, Neubrand A, Koch D. Characterization of hardness and stiffness of ceramic matrix composites through instrumented indentation test. Adv Eng Mater. 2018;21(5):1800806.

33. Lamon J. A micromechanics-based approach to the mechanical behavior of brittle-matrix composites. Compos Sci Technol. 2001;61(15):2259–72.

34. Chamis CC, Abdi F, Garg M, Minnetyan L, Baid H, Huang D, et al. Micromechanics-based progressive failure analysis prediction for WWFE-III composite coupon test cases. J Compos Mater. 2013;47(20–21):2695–712.

35. Lamon J. Approach to microstructure–behavior relationships for ceramic matrix composites reinforced by continuous fibers. In: Bansal NP, Lamon J editors. Ceramic matrix composites. Hoboken: John Wiley & Sons, Inc.; 2014: 520–47.